High-temperature behaviour of the helium-like Kα G ratio: the effect of improved recombination rate coefficients for calcium, iron and nickel

J. Oelgoetz,[1]★ C. J. Fontes,[1] H. L. Zhang,[1] M. Montenegro,[2] S. N. Nahar[2] and A. K. Pradhan[2]

[1]*Applied Physics Division, Los Alamos National Laboratory, PO Box 1663, MS F663, Los Alamos, NM 87545, USA*
[2]*Astronomy Department, the Ohio State University, 140 W. 18th Avenue, Columbus, OH 43210, USA*

ABSTRACT

It is shown that above the temperature of maximum abundance, recombination rates into the excited states of He-like ions that are calculated using earlier, more approximate methods differ markedly from rates obtained from recent distorted-wave and R-matrix calculations (unified recombination rate coefficients) for Ca, Fe and Ni. The present rates lead to G ratios that are greatly lower than those resulting from the more approximate rates in previous works, by up to a factor of 6 at high electron temperatures. Excellent agreement between the distorted-wave and the R-matrix rates, as well as excellent agreement in the G ratios calculated from them, provides support for the accuracy of these new values which have a broad applicability to the modelling and interpreting of X-ray spectra from a variety of astrophysical and laboratory sources.

Key words: atomic data – atomic processes – line: formation – X-rays: general.

1 INTRODUCTION

The Kα emission lines of He-like ions have been actively studied for quite some time, starting with Edlén & Tyrén (1939). Much of the basic theory and interpretation that is now used for astrophysical spectroscopy was established by Gabriel & Jordan (1969a) in their work to interpret solar spectra. While detailed discussions of the structure of the Kα complex and line ratios can be found elsewhere (see Gabriel & Jordan 1969a,b; Blumenthal, Drake & Tucker 1972; Gabriel 1972; Mewe & Schrijver 1978a,b; Pradhan & Shull 1981; Pradhan 1982), in brief there are four He-like lines in the Kα complex: $1s2p\,^1P_1 \rightarrow 1s^2\,^1S_0$ (w), $1s2p\,^3P_2 \rightarrow 1s^2\,^1S_0$ (x), $1s2p\,^3P_1 \rightarrow 1s^2\,^1S_0$ (y), $1s2s\,^3S_1 \rightarrow 1s^2\,^1S_0$ (z). The 'w' line is sometimes referred to as the resonance or dipole allowed line and 'y' as the intercombination line as it is dipole allowed through fine-structure mixing. The lines 'x' and 'z' both arise from higher order transitions, and as such are described by much slower rates. The 'x' line represents a magnetic quadrupole transition, and the 'z' line represents a magnetic dipole transition. Gabriel & Jordan (1969a) defined the temperature sensitive line ratio G as

$$G = \frac{I(x) + I(y) + I(z)}{I(w)}, \tag{1}$$

where $I(w)$ is the total emission in the 'w' line in units of number of photons $\text{cm}^{-3}\,\text{s}^{-1}$. In general, the behaviour of the G ratio is determined by the rate at which the He-like excited states are populated. At high temperatures these populations are determined

by an interplay between the processes of recombination and impact excitation. Recombination preferentially feeds the three lines arising from triplet states ('x', 'y' and 'z') while electron-impact excitation preferentially feeds the 'w' line. If the recombination rate is dominant, due, for example, to an increase in the number of H-like ions relative to the number of He-like ions, one would expect to see more flux in the 'x', 'y' and 'z' lines than in the 'w' line (as is observed in the case of recombining plasmas; Pradhan 1985; Oelgoetz & Pradhan 2004), resulting in a G ratio greater than one.

For heavier atoms the situation is more complex as satellite lines produced by radiative decay from autoionizing three-electron states are a prominent part of the Kα spectrum (see Gabriel & Jordan 1969b; Gabriel 1972; Mewe & Schrijver 1978a; Swartz & Sulkanen 1993; Bautista & Kallman 2000; Oelgoetz & Pradhan 2001 among others). These satellite lines become less important as temperature increases. As the high-temperature regime (above 10^7 K) is the interest of this present work, no investigation of line ratios involving satellite lines has been made, although we note that satellite lines can be, and often are, important at temperatures well above 10^7 K (Oelgoetz & Pradhan 2001). If the spectra are not adequately resolved, these satellite lines should be included in any line ratios used for analysis.

As this study investigates the effect of recombination rates [both radiative (RR) and dielectronic (DR)] on the high-temperature behaviour of the G ratio, a brief review of the data commonly used, how they are used and the reported high-temperature dependence of the G ratio is provided. CHIANTI (Dere et al. 1997; Landi et al. 2006), XSTAR (Bautista & Kallman 2001) and ATOMDB (Smith et al. 2001) are three commonly cited data bases in astrophysics. All three use different types of recombination data.

★E-mail: oelgoetz@lanl.gov

CHIANTI uses the recombination data of Mewe, Gronenschild & van den Oord (1985) for most He-like ions which is based on the work of Burgess & Seaton (1960) on recombination into neutral helium. The work of Mewe & Schrijver (1978a) is also based on Burgess & Seaton (1960) and has been used in some recent investigations such as Oelgoetz & Pradhan (2001) as well as the earlier work by Pradhan & Shull (1981). Fe and Ca are the exceptions to the above rule; for these elements CHIANTI uses the work by Bely-Dubau et al. (1982a,b) which is based on earlier studies of hydrogen by Burgess (1958). For completeness we note that Mewe et al. (1985) also depart from the above methodology and instead directly fit recombination data from Bely-Dubau et al. (1982a,b) for Fe XXV and Ca XIX. The hydrogenic methodology of Bely-Dubau et al. (1982a,b) has also been used in calculations for other elements (e.g. Porquet & Dubau 2000).

XSTAR takes a different approach; it calculates recombination rates from the photoionization cross-sections produced by the Opacity Project (Seaton 1987; Cunto et al. 1993), using more approximate methods only for $n > 10$. These Opacity Project cross-sections were calculated using R-matrix methods in LS coupling (Burke, Hibbert & Robb 1971; Berrington et al. 1987). Most recently, Oelgoetz & Pradhan (2004) used unified recombination rates based on R-matrix calculations (Nahar & Pradhan 1994) with relativistic fine structure included in the Breit–Pauli approximation.

ATOMDB uses the fits to distorted-wave photoionization data of Clark, Cowan & Bobrowicz (1986) for He-like cross-sections. These cross-sections are integrated to obtain the corresponding rates in the standard manner. Additionally, there are numerous individual calculations that use recombination rates from distorted-wave data in a similar fashion. Thus, much of the recombination data falls into three basic categories: data derived from more approximate methods (such as those by Burgess 1958; Burgess & Seaton 1960), data based on R-matrix calculations (Burke et al. 1971; Berrington et al. 1987) and data based on distorted-wave calculations.

Both Mewe et al. (1985) and Bautista & Kallman (2000) calculate the emission intensities of Fe XXV as does Pradhan & Shull (1981), using the Mewe & Schrijver (1978a) rate coefficients. If one calculates G ratios from the data presented in table IV of Mewe et al. (1985) the value of the G ratio is steadily decreasing, with values of approximately 0.5, in between 10^8 and 10^9 K. Pradhan & Shull (1981) show a G ratio taking a sharp upturn in the same temperature range and having a value greater than 1.0. Bautista & Kallman (2000) for this same temperature range report a G value in the range of 0.25 for Fe XXV, with a possibly slight rise as the electron temperature approaches 10^9 K. Thus the disagreement among these calculations is significant and resolving this discrepancy is the goal of the present work. To this end we use GSM (Oelgoetz 2006), a code recently developed to model plasma emission spectra, to explore the effects of different types of recombination data on the G ratio at high temperatures. Data from recent distorted-wave and R-matrix calculations are used and compared to rates calculated using expressions from Mewe & Schrijver (1978a) and Mewe et al. (1985); the exact rates in the XSTAR and ATOMDB data bases are not considered here. Additionally, only the effects of using different recombination data sets are explored while all other rates and the ionization balance are identical for all models of a particular element.

2 THEORY

GSM is a code based on the quasi-static approximation, that is the excited states of a given ion are considered to always be in equilibrium with the ground state of the ionization stage from which they arise,

and the neighbouring ionization stages (see Loch et al. 2004). GSM makes the additional approximation that some states can be treated purely as conduits that, through radiative decay or autoionization, allow population to transition into the final states of interest, thus neglecting the effect of collisions with these intermediate states. Both approximations are valid in the case of low-density plasmas where the radiation field can be neglected and are common to many of the previous calculations referenced in this work (see Gabriel & Jordan 1969a,b; Blumenthal et al. 1972; Gabriel 1972; Mewe & Schrijver 1978a,b; Pradhan & Shull 1981; Oelgoetz & Pradhan 2001, 2004).

As a consequence of these approximations the first step in any calculation is to solve for the total population of each ionization stage. This is done by solving the following set of coupled differential equations:

$$
\begin{aligned}
\frac{dX_i}{dt} = & \, N_e[X_{i+1}\alpha_{i+1\to i}(\tilde{\varepsilon}) + X_{i-1}C_{i-1\to i}(\tilde{\varepsilon})] \\
& + N_e^2[X_{i+1}\beta_{i+1\to i}(\tilde{\varepsilon}) - X_i\beta_{i\to i-1}(\tilde{\varepsilon})] \\
& - X_i N_e[\alpha_{i\to i-1}(\tilde{\varepsilon}) + C_{i\to i+1}(\tilde{\varepsilon})],
\end{aligned}
\tag{2}
$$

where X_i is the total population in the ith ionization stage, N_e the electron number density, $\tilde{\varepsilon}$ a variable that describes the shape of the electron distribution (in the case of this work $\tilde{\varepsilon}$ is the electron temperature as all results presented are for thermal systems with a Maxwellian distribution), C is a bulk collisional ionization rate coefficient, β a bulk three-body recombination rate coefficient and α a bulk recombination rate coefficient (which includes radiative and dielectronic recombination). Because all results presented in this work neglect the effect of a radiation field, photoionization and stimulated recombination have been omitted from equation (2). While GSM is capable of calculating these bulk rates by integrating the raw level-specific cross-sections and summing over all intermediate pathways, in general that approach would require a data set that is significantly larger than desired. As such these rates, when available, come from either tabulated or fitted data in the literature (such as can be found in Arnaud & Rothenflug 1985; Arnaud & Raymond 1992 or Mazzotta et al. 1998). All of the calculations presented in this study are steady-state calculations and therefore the left-hand side of equation (2) can be set to zero. We note that GSM is also explicitly designed to handle transient sources.

Once the total ionization stage populations have been calculated, they are used to calculate the individual level populations, and subsequently the spectra, by solving the following set of coupled equations:

$$
\begin{aligned}
\frac{dN_{l,j}}{dt} = & \, N_e\left\{ X_{l-1}\alpha^{\text{eff}}_{l-1,1\to l,j}(\tilde{\varepsilon}) - N_{l,j}\sum_i \alpha^{\text{eff}}_{j,l\to i,l+1}(\tilde{\varepsilon}) \right. \\
& + X_{l+1}C^{\text{eff}}_{l+1,1\to l,j}(\tilde{\varepsilon}) - N_{l,j}\sum_i C^{\text{eff}}_{l,j\to l-1,i}(\tilde{\varepsilon}) \\
& \left. + \sum_{i,i\neq j}\left[N_{l,i}q^{\text{eff}}_{i\to j}(\tilde{\varepsilon}) - N_{l,j}q^{\text{eff}}_{j\to i}(\tilde{\varepsilon}) \right] \right\} \\
& + N_e^2\left[X_{l-1}\beta^{\text{eff}}_{l-1,1\to l,j}(\tilde{\varepsilon}) - N_{l,j}\sum_i \beta^{\text{eff}}_{j,l\to i,l+1}(\tilde{\varepsilon}) \right] \\
& + \sum_{i,i>j}N_{l,i}A^{\text{eff}}_{i\to j} - N_{l,j}\sum_{i,i<j}A^{\text{eff}}_{j\to i} \\
& - N_{l,j}\sum_i R^{\text{AI-eff}}_{l,j\to i,l-1},
\end{aligned}
\tag{3}
$$

where the variables are defined more or less as before, with $N_{l,j}$ being the population in the jth state of the lth ionization stage, q^{eff} an

electron-impact (de-)excitation effective rate coefficient, $R^{\text{AI}-\text{eff}}$ an autoionization rate coefficient and A^{eff} an effective radiative decay rate. Just as in equation (2), (3) omits terms that involve the radiation field. It also omits excitation by proton and α particle impact, as they are neglected in this study for the sake of simplicity in order to better illustrate the effect of level-specific recombination rates on the G ratio. Once again all calculations consider steady-state conditions, so the left-hand side of equation (3) can be set to zero.

As mentioned earlier, GSM does not treat every spectroscopic level the same. Instead, it divides them into two categories: explicit (which are included as levels in equation 3, and coupled via all processes considered) and statistical (the effects of which are included when calculating the rate coefficients that go into equation 3). The inclusion of statistical states in the rate coefficients is accomplished via the collisionless transition matrix (CTM). A given element of the CTM can be thought of as the probability that once a statistical state gets populated, neglecting collisions, the atom or ion will end up in a given explicit state without passing through any other explicit states. If Q is the set of explicit states, the CTM can be defined using the following recursive expression:

$$
\begin{aligned}
T_{i \to j} = &\sum_{\substack{k \notin Q \\ (E_i > E_k > E_j)}} \frac{\Gamma_{i \to k}}{\sum_l A_{i \to l} + \sum_m R^{\text{AI}}_{i \to m}} T_{k \to j} \\
&+ \frac{\Gamma_{i \to j}}{\sum_l A_{i \to l} + \sum_m R^{\text{AI}}_{i \to m}},
\end{aligned}
\tag{4}
$$

where $\Gamma_{i \to k}$ is the appropriate type of spontaneous rate to connect i and k, via either radiative decay or autoionization. It should be noted that in order for this quantity to be meaningful, the state i must not be in the set Q.

After calculating the CTM, each effective rate coefficient can be constructed from the direct rate coefficient connecting the two explicit states and sums over all the indirect paths. For example effective collisional ionization rate coefficients are calculated as

$$
\begin{aligned}
C^{\text{eff}}_{i \to j}(\varepsilon) = &C^{\text{direct}}_{i \to j}(\varepsilon) + \sum_{\substack{k \\ (E_k > E_j)}} C^{\text{direct}}_{i \to k}(\varepsilon) T_{k \to j} \\
&+ \sum_{\substack{m \\ (E_m > 0)}} q^{\text{direct}}_{i \to m}(\varepsilon) T_{m \to j},
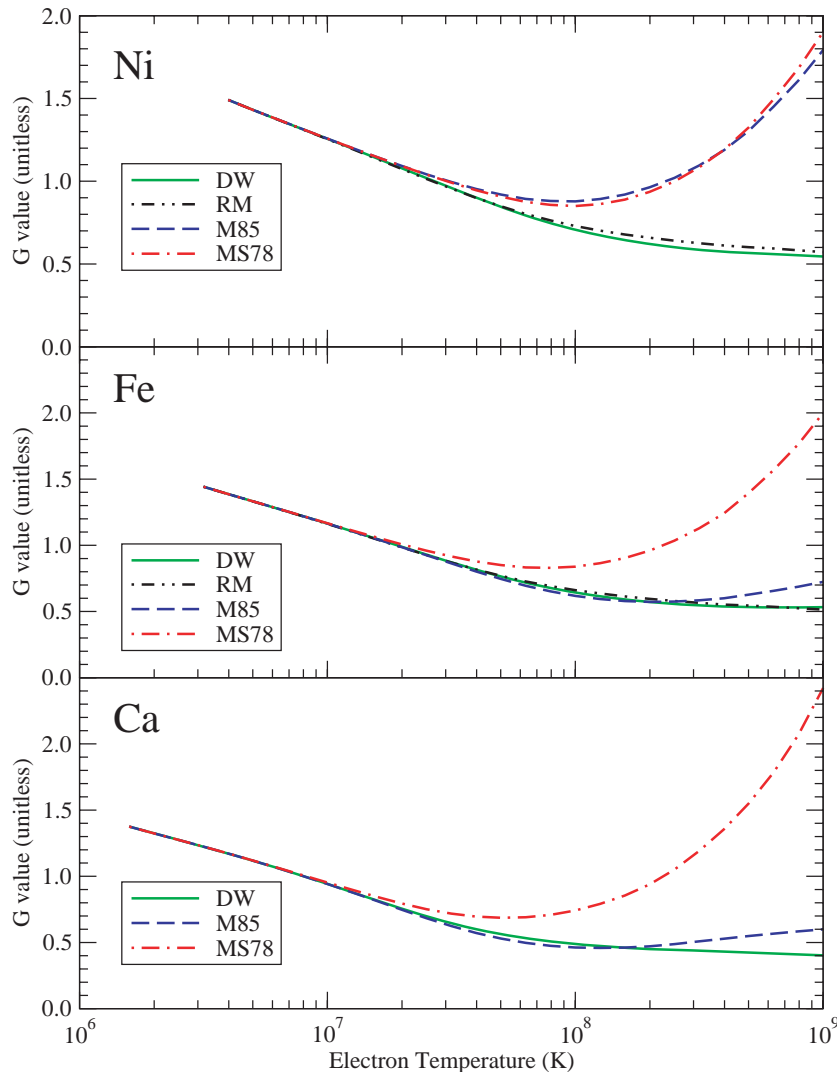\end{aligned}
\tag{5}
$$

Figure 1. G ratios for Ni (top), Fe (middle) and Ca (bottom) for each of the models considered.

recombination (RR+DR) rate coefficients as

$$\alpha_{j \rightarrow i}^{\text{eff}}(\varepsilon) = \alpha_{j \rightarrow i}^{\text{RR}}(\varepsilon) + D_{j \rightarrow i}^{\text{DC}}(\varepsilon) + \sum_{\substack{m \\ (E_m > E_i)}} \alpha_{j \rightarrow m}^{\text{RR}}(\varepsilon) \boldsymbol{T}_{m \rightarrow i}$$

$$+ \sum_{\substack{m \\ (E_m > E_j, E_m > E_i, E_m > 0)}} D_{j \rightarrow m}^{\text{DC}}(\varepsilon) \boldsymbol{T}_{m \rightarrow i}, \tag{6}$$

where D^{DC} is a dielectronic capture rate, and electron-impact excitation and de-excitation rate coefficients are calculated as

$$q_{j \rightarrow k}^{\text{eff}}(\varepsilon) = q_{j \rightarrow k}^{\text{direct}}(\varepsilon) + \sum_{\substack{l \\ (E_l > E_j, E_l > E_k)}} q_{j \rightarrow l}^{\text{direct}}(\varepsilon) \boldsymbol{T}_{l \rightarrow k}$$

$$+ \sum_{\substack{i \\ (E_i > E_j, E_i > E_k, E_i > 0)}} D_{j \rightarrow i}^{\text{DC}}(\varepsilon) \boldsymbol{T}_{i \rightarrow k}. \tag{7}$$

It should be noted that in equations (5)–(7) the effect of resonances are included as indirect pathways via terms involving dielectronic capture (D^{DC}). When R-matrix data are used, these terms are omitted to avoid double counting the effect of resonances.

Once equation (3) has been solved and the level populations obtained, synthetic spectra are calculated. The first step is to calculate the intensity (in number of photons $\text{cm}^{-3}\,\text{s}^{-1}$) of all lines in the desired energy range as

$$I(l, j \rightarrow l, k) = N_{l,j} A_{j \rightarrow k}. \tag{8}$$

Each line is then given a line shape corresponding to a thermal Doppler-broadened Gaussian profile. The total spectra, S, for a given photon energy, $h\nu$, can be expressed as

$$S(h\nu) = \sum_s I_s h\nu \frac{c\sqrt{m_i}}{2\pi kT} e^{[m_i c^2 (h\nu - \Delta E_{ij})^2]/(2\Delta E_{ij}^2 kT_i)}, \tag{9}$$

where s ranges over the set of all included transitions in the desired energy range, and the ion temperature, T_i, is taken to be equal to the electron temperature.

3 COMPUTATIONS

The baseline model considered in the present work uses the ionization balance data of Mazzotta et al. (1998) and detailed,
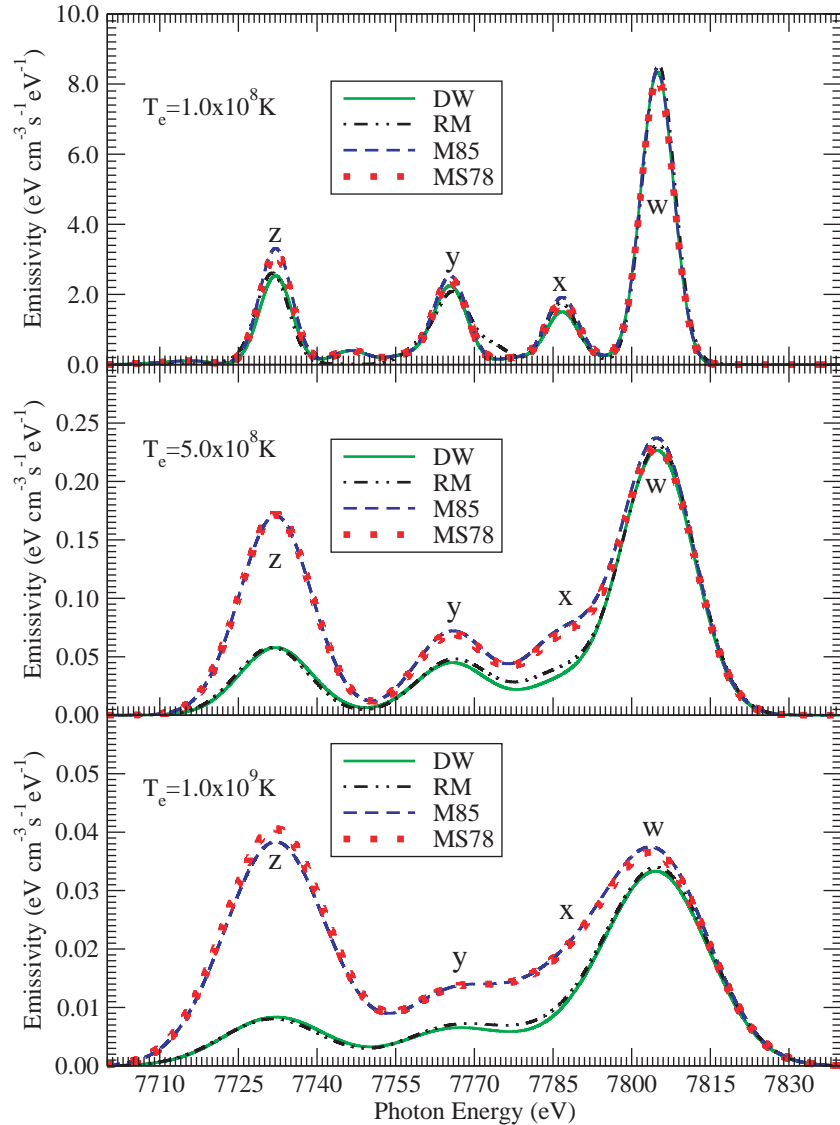

Figure 2. Emission spectra of a low-density ($N_e = 10^{10}\,\text{cm}^{-3}$) Ni plasma at three different temperatures in the high-temperature range where the G ratio from the models is in poor agreement. Spectra from the DW, M85 and MS78 models have all been redshifted by 9 eV to facilitate an easier comparison.

level-specific data calculated with the Los Alamos suite of atomic physics codes (see for instance Abdallah et al. 1994, 2001). The first step in such a calculation is to use the CATS code to calculate the bound and autoionizing wave functions, energies and dipole allowed radiative decay rates for all fine-structure levels arising from the configurations nl, $1snl$, $2lnl'$, $1s^{2nl}$, $1s2lnl'$ and $1s3lnl'$ with $n \leq 10$ and $l \leq g$ which span the H-like, He-like and Li-like ionization stages. Only fine-structure levels arising from the 1s, $1s^2$, $1s2l$, $1s^22l$ and $1s2lnl'$ configurations with $n \leq 10$ and $l \leq g$ were treated explicitly. All other levels were treated statistically. Convergence with respect to n was tested with a larger model that included up to $n \leq 20$. The GIPPER code is then used to calculate autoionization and photoionization cross-sections in the distorted-wave approximation, as well as collisional ionization cross-sections. As the ions under consideration are highly charged, a scaled hydrogenic approximation was used for collisional ionization cross-sections as it agrees well with distorted-wave results for systems such as these and is much more computationally efficient. The ACE code was used to calcu-

late distorted-wave cross-sections for all electron-impact excitation transitions out of the lowest seven levels of the He-like ionization stage, as well as the $1s^22l$ complex of the Li-like ionization stage (which is used to obtain effective collisional ionization rate coefficients into the He-like stage as well as a method for producing the Kα satellite lines). Lastly, the non-dipole A values that give rise to the 'x' and 'z' lines as well as a two-photon decay rate from $1s2\,^1S_0 \rightarrow 1s^2\,^1S_0$ were obtained from Mewe & Schrijver (1978a). All rates were calculated from these cross-sections inside of GSM. We refer to this baseline model as DW.

The second model, which is designated RM, begins with the first model and replaces the radiative and dielectronic recombination data from the H-like ionization stage into the He-like ionization stage with total and level-specific rate coefficients for recombination into all fine-structure levels SLJ with $n \leq 10$ calculated from Breit–Pauli R-matrix photoionization cross-sections (Nahar & Pradhan 1994). While there are unified recombination data available in the literature for Ni (Nahar 2005) and Fe (Nahar, Pradhan & Zhang
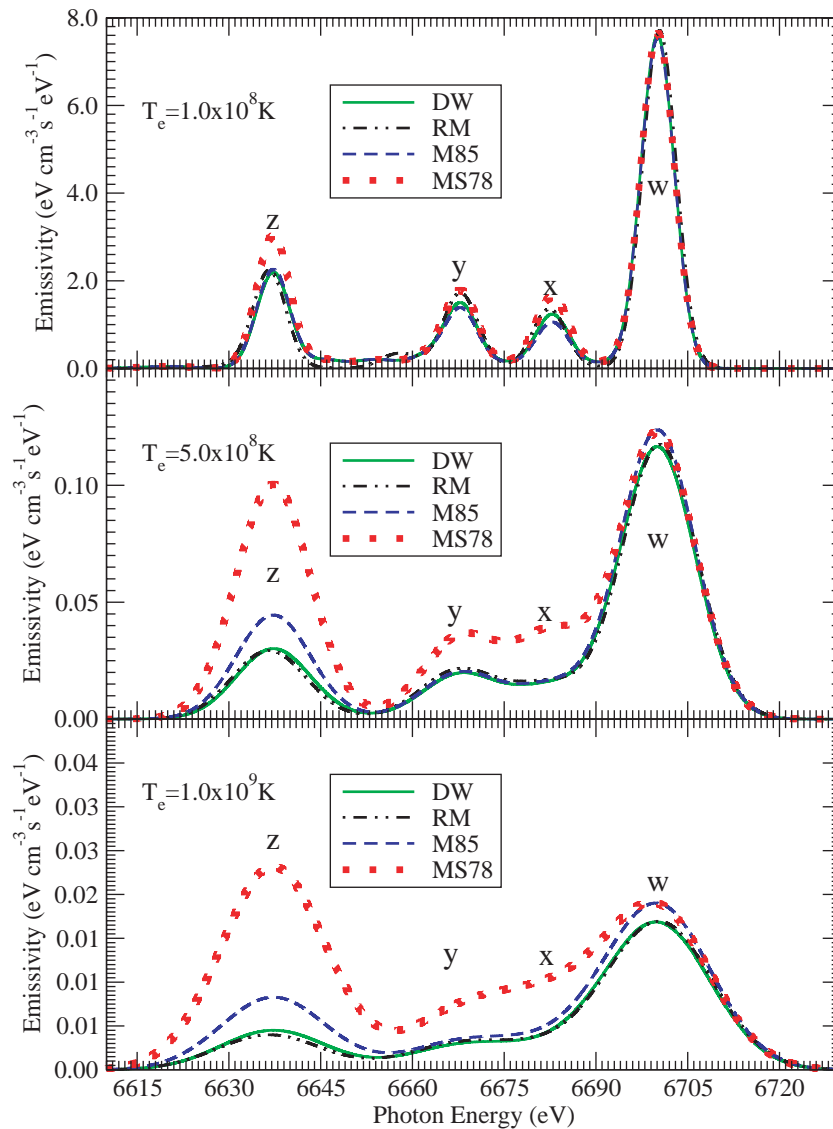

Figure 3. Emission spectra of a low-density ($N_e = 10^{10}$ cm^{-3}) Fe plasma at three different temperatures in the high-temperature range where the G ratio from the models is in poor agreement. Spectra from the DW, M85 and MS78 model have all been redshifted by 7 eV to facilitate an easier comparison.

2001), we do not consider a Ca, RM model as there are no data yet available for this species. In addition, the energy levels and radiative decay rates inside the He-like ion are replaced by R-matrix data (the radiative decay rates are taken from Nahar & Eissner, in preparation for Ni and Nahar & Pradhan 1999 for Fe). Lastly, the unified recombination rates through a given satellite line of Nahar & Pradhan (2006) are used to calculate the dielectronic recombination contribution to the intensity of all the *KLL* satellite lines in this model.

The third model, referred to as M85, also begins with the baseline model and replaces the recombination rates from the H-like ionization stage into the He-like excited states with rates calculated using the expressions of Mewe et al. (1985). These expressions are fits to previously published data. In the case of Ni, the fits are to the rates of Mewe & Gronenschild (1981), which are based on the work of Burgess & Seaton (1960) concerning the recombination of neutral He. These fits do not include the contribution of dielectronic recombination, so in the Ni M85 model dielectronic recombination is included using the data from the baseline DW model. Mewe et al. (1985) fit the data of Bely-Dubau et al. (1982a) for Fe and Bely-Dubau et al. (1982b) for Ca. Both of these works are based on

the hydrogenic recombination work of Burgess (1958). It should be noted that Bely-Dubau et al. (1982a,b) only present rates up to an electron temperature of 10^8 K. As such, using the fits of Mewe et al. (1985) to these data beyond this temperature may exceed the range of validity intended by Bely-Dubau et al. (1982a,b). Furthermore, these rates do include the effect of dielectronic recombination, so this contribution is not recalculated and included a second time by GSM.

The fourth model, MS78, is much like the third, but instead calculates radiative recombination rates using the expressions of Mewe & Schrijver (1978a), which are also based on the work of Burgess & Seaton (1960). As these rates do not include dielectronic recombination, this model includes DR rates obtained from the data contained in the baseline, DW model.

4 RESULTS

The results for the *G* ratio for all models under consideration are presented in Fig. 1. The differences are striking. As temperature increases and recombination becomes more important to spectral
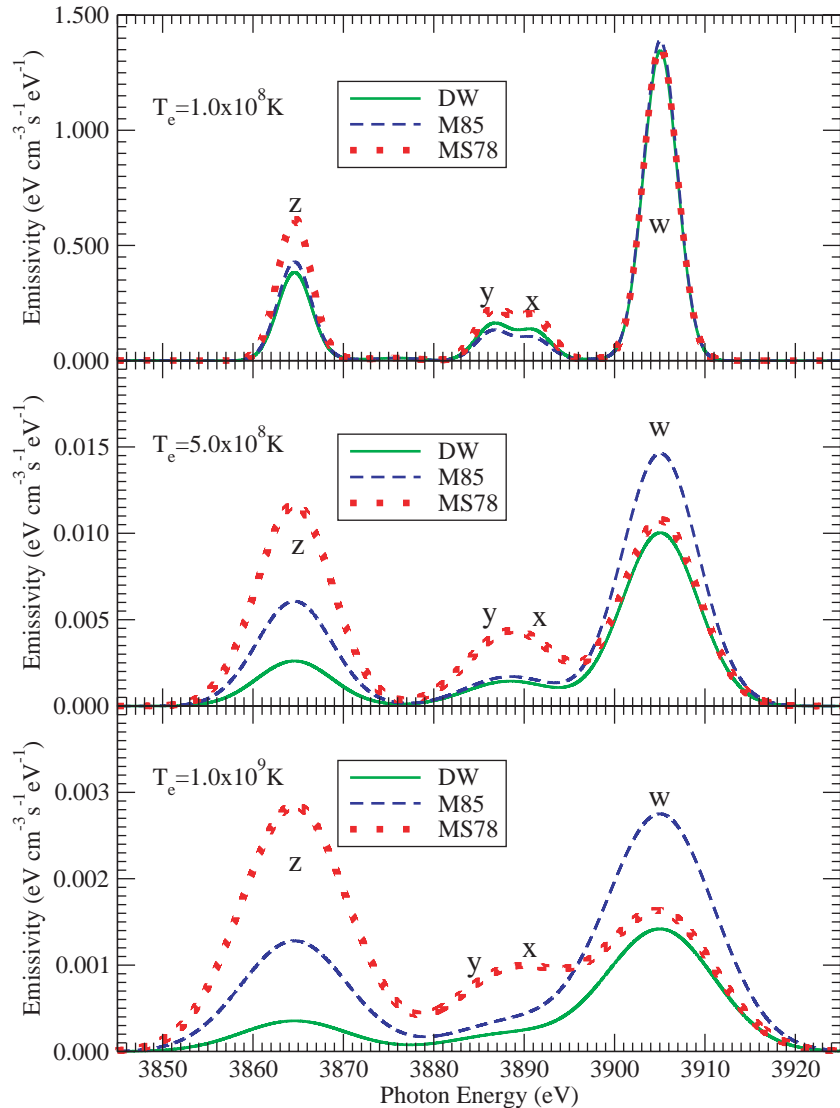

Figure 4. Emission spectra of a low-density ($N_e = 10^{10}$ cm^{-3}) Ca plasma at three different temperatures in the high-temperature range where the *G* ratio from the models is in poor agreement.

formation, the more approximate rates of Mewe & Schrijver (1978a) produce *G* ratios that diverge significantly from the results obtained with the newer DW and RM models for all three elements. The M85 result for Ni displays similar discrepancies while the M85 results for Fe and Ca (which are fits to Bely-Dubau et al. 1982a,b) agree better with the RM and DW models. Not surprisingly (given the highly charged nature of these systems) the RM and DW models are in excellent agreement at all temperatures.

Upon investigation of the underlying spectra (Figs 2–4) to find the source of the divergence in predicted *G* values at high temperature, one continues to see excellent agreement at all temperatures between the RM and DW models; but the analysis is not as straightforward for the more approximate methods. In the case of Ni (Fig. 2), both the M85 and MS78 model agree well with each other, predicting significantly more flux in the 'x', 'y' and 'z' lines, and slightly more flux in the 'w' line, at high temperatures than either of the more accurate models. This behaviour is consistent with the fact that both models are based on the same underlying work by Burgess & Seaton (1960). The spectrum for Fe (Fig. 3) is more interesting

because, while the MS78 model continues to predict significantly stronger 'x', 'y' and 'z' lines, and a slightly stronger 'w' line, compared to the DW and RM models, the M85 model predicts a rather different result. Like the MS78 model, the M85 model predicts a slightly stronger 'w' line, but the 'z' line is in much better agreement with the DW and RM models than the MS78 model. Furthermore, the M85 model does a good job of predicting the 'x' and 'y' line intensities.

The detailed results for Ca (Fig. 4) are somewhat similar to those presented for Fe. The MS78 model continues to predict much stronger 'x', 'y' and 'z' lines when compared to the DW data set and only a slightly stronger 'w' line. The M85 model is in good agreement for the 'x' and 'y' lines and much closer for the 'z' line, but in the case of Ca it predicts a much stronger 'w' line. This overprediction tends to mitigate the effect of the enhanced 'z' line, producing a fortuitously lower value for the *G* ratio. This type of cancellation underscores the importance of examining the actual spectra to gain a better understanding of the quality of the underlying atomic data.
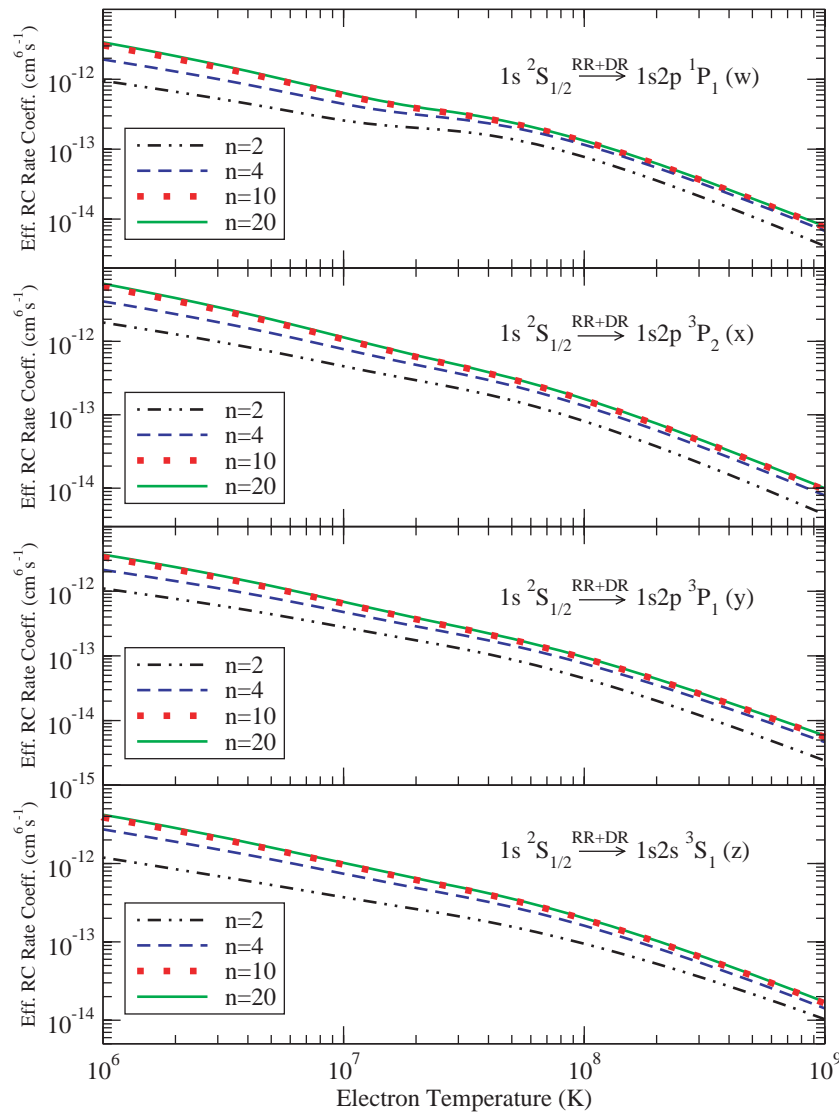

Figure 5. Four effective recombination rate coefficients for Fe as a function of the highest principal quantum number included in the DW model. Of particular interest is how quickly the rate coefficient converges in the high-temperature region due to cascade terms becoming less important.

In order to determine the fundamental reasons behind the above discrepancies in the spectra and G ratios, the recombination rates must be examined in detail, but first it is useful to ensure that the models are large enough (as a function of the principal quantum number n) to have converged upon the correct answer. As the various sources cited in this work all chose different limits for the maximum n value used in their calculations, lack of convergence could be a reason for the differences. Additionally, such a study can be used to investigate the relative importance of cascade corrections, which Pradhan & Shull (1981) suggested to be the cause of the upturn in the G ratio displayed in that work. As the results for each element are very similar, only recombination rate coefficients for Fe are presented (Fig. 5) and discussed for only the DW model.

In Fig. 5 it can be seen that by $n = 10$ the effective rate coefficients into the relevant four spectroscopic levels have converged to within ~5 per cent when the temperature is above 10^8 K. All models considered in this work extend at least this far in principal quantum number; thus, the extent of the model (in n) is not the cause of the

discrepancies. Of additional note is the fact that Fig. 5 indicates that recombination cascades become less important (as a method of populating the He-like excited states) at higher temperatures, even as recombination is becoming a more important process for the population of He-like excited states. According to the analysis of the DW model, it is the direct recombination rate that is the most important process at higher temperatures while cascades play a progressively smaller role.

Moving on to a comparison of the effective recombination rate coefficients in the four models (again presented only for Fe since the Ca and Ni results show similar trends) shown in Fig. 6, there are obvious discrepancies at high temperatures and the cause of the differences in simulated spectra becomes evident. The two more approximate models (MS78 and M85) are in reasonable agreement with the more accurate DW and RM models in the middle-temperature region. Outside the range, there is a marked difference (as much as a factor of 5 in the high-temperature region). This difference in the recombination rate coefficients in the high-temperature regime is responsible for the corresponding difference
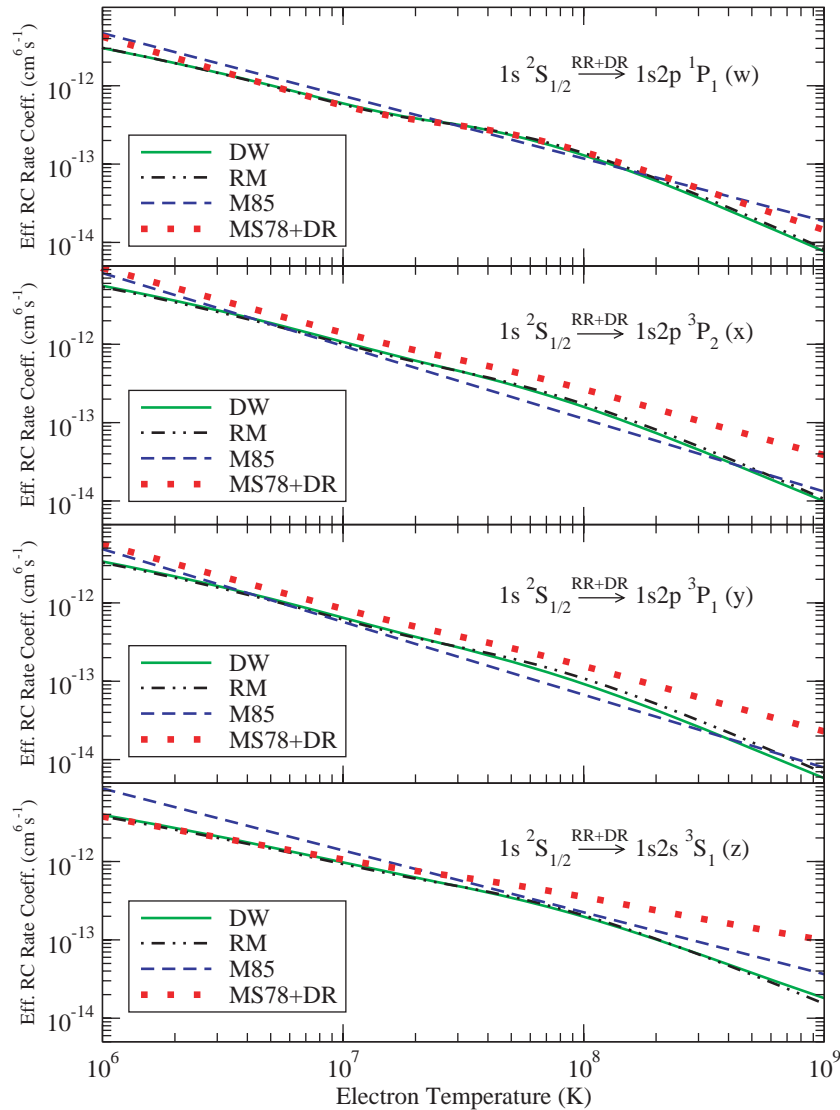

Figure 6. Comparison of the effective recombination rate coefficients for Fe for the various models. Of particular note are the large discrepancies at electron temperatures above 10^8 K.

in the *G* ratio among the various calculations. The values of the new DW and RM recombination data are significantly smaller than the MS78 data, which result in decreased recombination rates for populating the 'x', 'y' and 'z' lines, while the impact-excitation rate for feeding the 'w' line remains essentially fixed for each type of calculation. Thus, the reduced DW and RM recombination data cause a delay in the onset of any increase in the *G* ratio to a higher temperature, resulting in the large differences displayed in Fig. 1.

It should be noted that Nahar et al. (2001) saw a similar difference in the recombination rates in the high-temperature region when they compared their level-specific unified recombination rates with the direct component of the recombination rate expressions of Mewe & Schrijver (1978a). Again there is excellent agreement between the DW and RM models over the entire temperature range, bolstering confidence in their validity.

5 CONCLUSION

While the results of calculations using recombination rates derived from more accurate and extensive distorted-wave and R-matrix calculations agree quite well, both disagree significantly with the previous, more approximate calculations of Mewe & Schrijver (1978a), Mewe & Gronenschild (1981), Bely-Dubau et al. (1982a,b) and Mewe et al. (1985). The results obtained from models based on the more accurate distorted-wave and R-matrix data show a continually decreasing *G* ratio over the investigated temperature range. This behaviour disagrees strongly with the sharp upturn observed at high temperatures in the *G* ratios calculated from the more approximate models. The discrepancy is up to a factor of 6 in the *G* ratio (see Fig. 1), and was determined to be caused by large differences in the recombination contributions. The more approximate rates produce results that agree reasonably well with the newer DW and RM data up to approximately 10^8 K, but can lead to unphysical values when used outside of this range.

Further work is required to refine and verify calculations of the *G* ratio and the underlying data from which it is determined. Studies similar to the present one are needed, but including electron-impact excitation rates as well as collisional ionization rates from the ground state of the Li-like species into the excited states of the He-like species. Investigation of the effect of the ionization balance may also be required. These studies are underway.

ACKNOWLEDGMENTS

REFERENCES

Abdallah J., Jr, Clark R. E. H., Peek J. M., Fontes C. J., 1994, J. Quant. Spectrosc. Radiat. Transfer, 51, 1
Abdallah J., Jr, Zhang H. L., Fontes C. J., Kilcrease D. P., Archer B. J., 2001, J. Quant. Spectrosc. Radiat. Transfer, 71, 107
Arnaud M., Raymond J., 1992, ApJ, 398, 394
Arnaud M., Rothenflug R., 1985, A&AS, 60, 425
Bautista M. A., Kallman T. R., 2000, ApJ, 544, 581
Bautista M. A., Kallman T. R., 2001, ApJS, 134, 139
Bely-Dubau F., Faucher P., Dubau J., Gabriel A. H., 1982a, MNRAS, 198, 239
Bely-Dubau F. et al., 1982b, MNRAS, 201, 1155
Berrington K. A., Burke P. G., Butler K., Seaton M. J., Storey P. J., Taylor K. T., Yan Y., 1987, J. Phys. B: At. Mol. Phys., 20, 6379
Blumenthal G. R., Drake G. W. F., Tucker W. H., 1972, ApJ, 172, 205
Burgess A., 1958, MNRAS, 118, 477
Burgess A., Seaton M. J., 1960, MNRAS, 121, 471
Burke P. G., Hibbert A., Robb W. D., 1971, J. Phys. B: At. Mol. Phys., 4, 153
Clark R. E. H., Cowan R. D., Bobrowicz F. W., 1986, At. Data Nucl. Data Tables, 34, 415
Cunto W., Mendoza C., Ochsenbein F., Zeippen C. J., 1993, A&A, 275, L5
Dere K. P., Landi E., Mason H. E., Monsignori Fossi B. C., Young P. R., 1997, A&AS, 125, 149
Edlén B., Tyrén F., 1939, Nat, 143, 940
Gabriel A. H., 1972, MNRAS, 160, 99
Gabriel A. H., Jordan C., 1969a, MNRAS, 145, 241
Gabriel A. H., Jordan C., 1969b, Nat, 221, 947
Landi E., Del Zanna G., Young P. R., Dere K. P., Mason H. E., Landini M., 2006, ApJS, 162, 261
Loch S. D., Fontes C. J., Colgan J., Pindzola M. S., Ballance C. P., Griffin D. C., O'Mullane M. G., Summers H. P., 2004, Phys. Rev. E, 69, 066405
Mazzotta P., Mazzitelli G., Colafrancesco S., Vittorio N., 1998, A&AS, 133, 403
Mewe R., Gronenschild E. H. B. M., 1981, A&AS, 45, 11
Mewe R., Schrijver J., 1978a, A&A, 65, 99
Mewe R., Schrijver J., 1978b, A&A, 65, 115
Mewe R., Gronenschild E. H. B. M., van den Oord G. H. J., 1985, A&AS, 62, 197
Nahar S. N., 2005, ApJS, 158, 80
Nahar S. N., Pradhan A. K., 1994, Phys. Rev. A, 49, 1816
Nahar S., Pradhan A., 1999, A&AS, 135, 347
Nahar S. N., Pradhan A. K., 2006, Phys. Rev. A, 73, 062718
Nahar S. N., Pradhan A. K., Zhang H. L., 2001, ApJS, 133, 255
Oelgoetz J., 2006, PhD thesis, The Ohio State University
Oelgoetz J., Pradhan A. K., 2001, MNRAS, 327, L42
Oelgoetz J., Pradhan A. K., 2004, MNRAS, 354, 1093
Porquet D., Dubau J., 2000, A&A, 143, 495
Pradhan A. K., 1982, ApJ, 263, 477
Pradhan A. K., 1985, ApJ, 288, 824
Pradhan A. K., Shull J. M., 1981, ApJ, 249, 821
Seaton M., 1987, J. Phys. B: At. Mol. Phys., 20, 6363
Smith R. K., Brickhouse N. S., Liedahl D. A., Raymond J. C., 2001, ApJ, 556, L91
Swartz D. A., Sulkanen M. E., 1993, ApJ, 417, 487

This paper has been typeset from a TEX/LATEX file prepared by the author.